

Flywheel Inverted Pendulum Design for Evaluation of Swing-Up Energy-Based Strategies

Victor G. Cardoso * Thiago F. F. de Souza * Pedro M. G. del Foyo *

* *Departamento de Engenharia Mecânica, Universidade Federal de Pernambuco, PE, (e-mails: victor.cardoso@ufpe.br, thiago.fsouza@ufpe.br, pedro.foyo@ufpe.br).*

Abstract: Inverted pendulums are an important class of underactuated systems. This paper presents a flywheel inverted pendulum (FIP) design to evaluate the performance of Swing-up and Balance control algorithms. The Swing-up algorithms evaluated are based on Energy Control strategies. The rise time and an estimation of the energy spent on this task were used as assessment metrics. Two closed loops with PID controllers were implemented to perform the Balance control of the FIP. The analyses were carried out based on the data generated from simulations and experiments. The results showed that the Maximum Energy algorithm was able to perform the swing-up with less time and lower energy consumption. Additionally, it resulted in lower errors during the execution of the Balance control, since the system conditions provided by this swing-up strategy contributed to the robustness of the system.

Keywords: Flywheel Inverted Pendulum; Swing-up Control; Energy Control; Balance Control.

1. INTRODUCTION

By definition, an inverted pendulum is a mechanical system which its center of mass is located above the pivot point. In order to drive and keep the system at the equilibrium position, it is necessary to add energy accordingly to the system. This mechanism is extensively studied due to its applications in many engineering areas, including Robotics (Dai et al., 2015), Oil and Gas technologies (Kareem, 1983) and Aerospace Engineering (Ferrante, 2017). Additionally, due to the simplicity on their operating principles, it is a remarkable underactuated non-linear system commonly used as case study for control techniques analysis for academic purposes. One of the most exploited designs in the literature is called the Flywheel Inverted Pendulum (FIP). This mechanism is based on a motor attached to a flywheel, located at the end of the rod, that uses the physical principle of conservation of mechanical energy to control the system properly.

The standard operation of a flywheel inverted pendulum is mainly based on two stages: the Swing-up control and the Balance control (Srinivas and Behera, 2008). The Swing-up control consists in taking the pendulum from the downright to the upright position. When the pendulum reaches certain conditions (normally, when a small angle around of the vertical position is achieved) it is possible to switch to the Balance control, which is responsible to keep the pendulum in the vertical position as long as possible.

The behavior of the working stages are strictly related to the physical parameters of the FIP. Therefore, there are several works in the literature that uses the analytical model of the plant to design a satisfactory controller to meet the project requirements. Olivares and Albertos (2013) presented a balance control architecture based on a simplified linear model derived from a prototype, that

utilizes two control loops in order to reach a good performance. Nguyen and Huynh (2016) combined Olivares' approach to a current control method to obtain even better results regarding the balance control of a FIP.

Balance control was explored in different ways by the authors. Many works have presented solutions with non-linear controllers (Spong et al., 2001), (Teja et al., 2020), (Trentin et al., 2020). However, these implementations tend to be complex and may require the use of more sensors in the system. On the other hand, using simpler linear control architectures, such as PID controllers, proved to be quite effective for various scenarios (Olivares and Albertos, 2013), (Vasconcelos et al., 2019), (Almada et al., 2020).

Regarding the Swing-up, strategies based on Energy Control (EC) are widely present in related works. One of its main features is to control the energy of the system instead of directly controlling its position or velocity (Åström and Furuta, 2000). Many authors focused on proposing solutions for enhancing the Swing-up performance in comparison with Energy control implementations. Åström and Furuta (2000) presented a comparison between these strategies and minimum time solutions. Srinivas and Behera (2008) introduced two novel strategies and compared their performance with Energy control based algorithms.

This work aims to analyze the behavior of two Swing-up strategies based on Energy Control. A Balance Control algorithm will also be implemented. Experiments will be carried out in a simulation environment and in a real FIP. The Swing-up rise time, an estimation of the energy demanded by each strategy and the integration of the error during the Balance Control will be used as metrics for assessing the experiments.

This paper is organized as follows. Section 2 contains the deduction of a analytical model of a FIP and presents

technical details about the FIP built for this work. Section 3 describes the system identification method applied, the strategies proposed for Swing-up and Balance control algorithms. Section 4 shows the main results accomplished by the analysis and a brief discussion of them. The conclusions are presented in Section 5.

2. FLYWHEEL INVERTED PENDULUM

2.1 Analytical Model

Modelling a FIP combines the characteristic parameters of the actuator with the physical laws that rules the system behavior. In this work, a DC motor is considered as actuator and it can be described as:

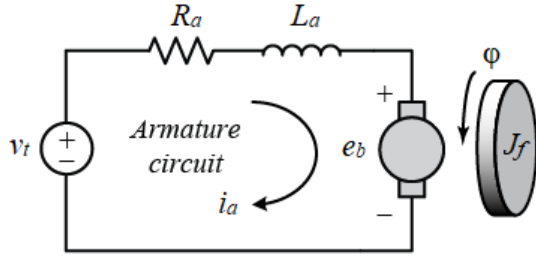


Figure 1. DC Motor - physical model.

where v_t is the input voltage, R_a and L_a are the armature resistance and inductance, respectively, e_b is the back electromotive force and φ is the rotor angle. Neglecting the armature inductance and applying the Kirchhoff's voltage law, we have:

$$R_a i_a + e_b = v_t \quad (1)$$

The armature current and the back electromotive force can be expressed in terms of motor torque (τ_m) and motor speed ($\dot{\varphi}$), respectively.

$$e_b = K_1 \dot{\varphi} \quad (2)$$

$$\tau_m = K_2 i_a \quad (3)$$

Substituting the equations (2) and (3) into (1), we obtain:

$$\frac{R_a}{K_2} \tau_m + K_1 \dot{\varphi} = v_t \quad (4)$$

The torque developed by the motor is counterbalanced by the flywheel moment of inertia. Neglecting the friction on the motor shaft we have the following dynamic equations of the motor:

$$\tau_m = J_f \ddot{\varphi} \quad (5)$$

Replacing τ_m in (4) by (5), we have:

$$\frac{J_f R_a}{K_2} \ddot{\varphi} + K_1 \dot{\varphi} = v_t \quad (6)$$

Rearranging (6):

$$\ddot{\varphi} + \frac{K_1 K_2}{R_a J_f} \dot{\varphi} = \frac{K_2}{R_a J_f} v_t \quad (7)$$

The free body diagram of the FIP is presented in Figure 2. Table 1 shows the meaning of each term in the image. Analyzing the free body diagram of the system, it is

possible to obtain an equation that express the relation between reaction wheel rotation with the pendulum's kinetics properties.

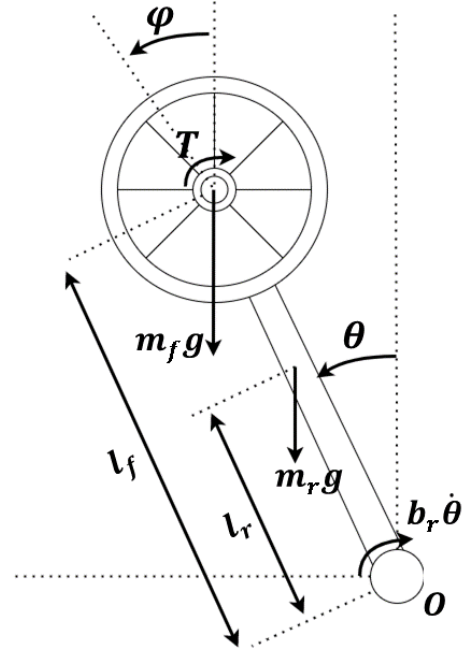


Figure 2. Flywheel Inverted Pendulum - physical model.

$$(J - J_f) \ddot{\theta} = -T + (m_r l_r + m_f l_f) g \sin(\theta) - b_r \dot{\theta} \quad (8)$$

The torque shown in Figure 2, represents the torque acting on the pendulum, which is the opposite of the torque acting on the rotor. Noting that $T = J_f \ddot{\varphi}$ and assuming $\sin(\theta) \approx \theta$ for small pendulum oscillations around the reference point, we get an approximate linear model for the dynamics of the inverted pendulum dynamics:

$$(J - J_f) \ddot{\theta} + J_f \ddot{\varphi} - MLg\theta + b_r \dot{\theta} = 0 \quad (9)$$

where $ML = m_r l_r + m_f l_f$. Around the natural position, i.e., when the pendulum is hanging in the downward equilibrium, there is an inversion on the sign of θ term because $\sin(\theta + 180^\circ) = -\sin(\theta) \approx -\theta$ for small variations of θ . Hence:

$$(J - J_f) \ddot{\theta} + J_f \ddot{\varphi} + MLg\theta + b_r \dot{\theta} = 0 \quad (10)$$

Table 1. Description of terms of the FIP physical model.

Var	Description
θ	Pendulum angle
φ	Flywheel angle
b_m	Viscous friction coefficient of the motor
b_r	Viscous friction coefficient of the rod axis of rotation
g	Gravity acceleration
m_r	Rod mass
m_f	Flywheel mass + motor mass
l_r	Distance from the rotation axis to rod center mass
l_f	Distance from the rotation axis to flywheel center mass
J_r	Moment of inertia of the rod around its center mass
J_f	Moment of inertia of the flywheel around its center mass
J	Moment of inertia of the pendulum around O axis

The transfer function for this model correlates the pendulum angle (θ) with the voltage input (v_t) in the frequency domain. The Laplace transform of (6) and (10) were used to obtain the transfer function of the system.

$$\frac{\Theta(s)}{\Phi(s)} = \frac{-\frac{J_f}{J-J_f} s^2}{s^2 + \frac{b_r}{J-J_f} s + \frac{MLg}{J-J_f}} \quad (11)$$

$$\frac{\Phi(s)}{V_t(s)} = \frac{\frac{K_2}{R_a J_f}}{s^2 + \frac{K_1 K_2}{R_a J_f}} \quad (12)$$

Combining (11) and (12), we get to the linear transfer function of the system in the natural position, described as:

$$\frac{\Theta(s)}{V_t(s)_{natural}} = \frac{-\frac{K_2}{R_a(J-J_f)} s}{s^3 + K_{rm} s^2 + \left(K_r K_m + \frac{MLg}{J-J_f}\right) s + \frac{MLg K_m}{J-J_f}} \quad (13)$$

where:

$$\begin{aligned} K_{rm} &= K_r + K_m \\ K_r &= \frac{b_r}{J - J_f} \\ K_m &= \frac{K_1 K_2}{R_a J_f} \end{aligned}$$

2.2 State Space Representation

The state space representation used to model this system was based on the linearized version of the FIP at the upright position. To do so, the state variables were defined as: $x_1 = \theta$, $x_2 = \dot{\theta}$ and $x_3 = \dot{\varphi}$. Isolating the first derivative of the state variables of equations (7) and (9), we obtain the following equations:

$$\begin{aligned} \dot{x}_1 &= x_2 \\ \dot{x}_2 &= \frac{MLg}{J - J_f} x_1 - K_r x_2 + \frac{K_m J_f}{J - J_f} x_3 - \frac{K_2}{R_a (J - J_f)} u \\ \dot{x}_3 &= -K_m x_3 + \frac{K_2}{R_a J_f} u \end{aligned} \quad (14)$$

Expressing the previous equations in the matrix form, the state space representation of the FIP is given by:

$$\begin{bmatrix} \dot{x}_1 \\ \dot{x}_2 \\ \dot{x}_3 \end{bmatrix} = \begin{bmatrix} 0 & 1 & 0 \\ \frac{MLg}{J-J_f} & -K_r & \frac{K_m J_f}{J-J_f} \\ 0 & 0 & -K_m \end{bmatrix} \begin{bmatrix} x_1 \\ x_2 \\ x_3 \end{bmatrix} + \begin{bmatrix} 0 \\ -\frac{K_2}{R_a (J-J_f)} \\ \frac{K_2}{R_a J_f} \end{bmatrix} u \quad (15)$$

$$y = [1 \ 0 \ 0] \begin{bmatrix} x_1 \\ x_2 \\ x_3 \end{bmatrix} \quad (16)$$

2.3 FIP Construction

The designed prototype for the experimental tests was implemented using a DC motor (model: Chihai GM25-370 2000rpm), powered with 12V, attached to a reaction wheel manufactured in PLA plastic. The rod was also made by 3D printing and its rotation axis is attached to an angle sensor (Hall effect potentiometer, model P3022-V1-CW360). An Arduino Uno board was used for data acquisition, control and communication tasks. The mechanical structure was built using aluminum and wood pieces. The 3D model and the real prototype are shown in Figures 3 and 4, respectively.

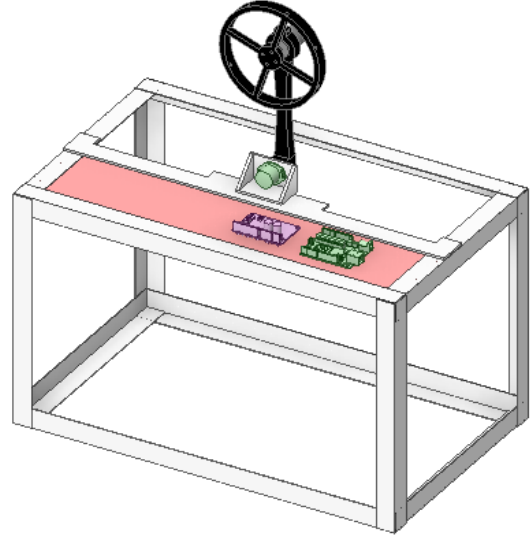


Figure 3. Flywheel Inverted Pendulum 3D model.

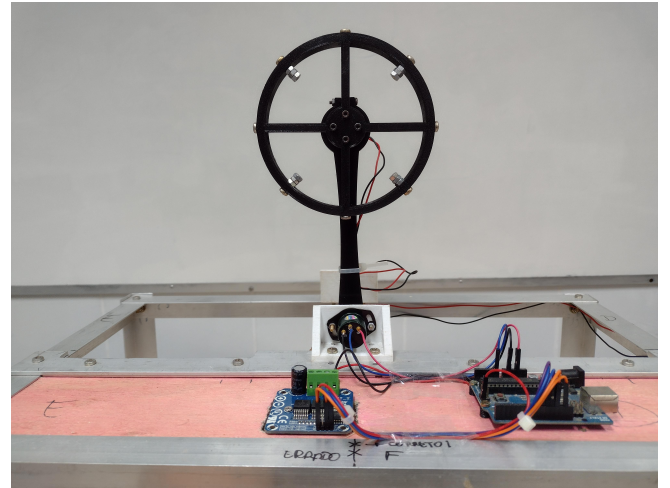


Figure 4. Flywheel Inverted Pendulum prototype.

3. METHODOLOGY

3.1 System Identification

In order to estimate the unknown parameters of the non-linear model (6) and (8), experiments were carried out to obtain the parameters of the linear transfer function (13). The system identification method utilized in this

paper was based on the steps described by Vasconcelos et al. (2019). The transfer function exported by this method is corresponding to the natural version because the experiments were run when the FIP was around the downright position. Once the unknown parameters have been estimated, it is possible to determine all terms in the transfer function of the pendulum at the inverted position (17). This equation was obtained considering (9) instead of (10) on transfer function deduction. Hence, the resulting equation is:

$$\frac{\Theta(s)}{V_t(s)_{inverted}} = \frac{-\frac{K_2}{R_a(J-J_f)}s}{s^3 + K_{rm}s^2 + \left(K_r K_m - \frac{MLg}{J-J_f}\right)s - \frac{MLgK_m}{J-J_f}} \quad (17)$$

Although the parameters involving masses and lengths can be measured directly, it is still necessary to find the values of the constants K_r , K_m and J to have a full description of the functions. To determine these terms, the system identification methodology adopted was based on applying a known input signal to the system at the natural position and record the output data for a period of time. In our case, a step function was applied as input signal and the pendulum angle response was recorded. This experiment was run five times and at each time, a different amplitude for the step signal was utilized. All experiments had the same time duration: 60 seconds, with sample frequency of 50Hz.

After collecting all the experimental data, the *System Identification Toolbox*, of the *Matlab* software, was used to estimate the candidate models. The search was constrained in finding transfer functions containing 1 zero and 3 poles, as observed from the analytical model. The transfer functions found with the best fits are shown in Table 2.

Table 2. Percentage accuracy of the models obtained from the experiments.

	Ex. 1	Ex. 2	Ex. 3	Ex. 4	Ex. 5	Avg
$G_1(s)$	77.74	76.88	59.26	71.14	69.08	70.82
$G_2(s)$	72.14	83.85	70.67	84.37	83.49	78.90
$G_3(s)$	58.62	70.52	87.69	76.91	78.67	74.48
$G_4(s)$	67.23	80.95	77.40	89.22	90.95	81.15
$G_5(s)$	65.49	79.77	78.37	88.93	91.42	80.80

The transfer function $G_4(s)$ had the best average percentage accuracy among all the candidates. Therefore, it was chosen to drive the estimation for the unknown parameters of (13) and (17).

$$G_4(s) = \frac{-1.511s + 0.046}{s^3 + 7.359s^2 + 66.09s + 455} \quad (18)$$

However, the equation (18) has some terms that does not exist in the analytical model. Thus, these terms were disregarded and the impact of this removal was assessed. The adapted transfer function is expressed by:

$$G_{4mod}(s) = \frac{-1.511s}{s^3 + 7.359s^2 + 66.09s + 455} \quad (19)$$

The adapted transfer function has been validated with the experimental data collected previously, and it achieved

80.75% of accuracy on average. It preserved the good results presented by the original equation, G_3 .

Comparing equations (13) and (19), we find:

$$\begin{cases} K_r + K_m = 7.359 \\ K_r K_m + \frac{MLg}{J-J_f} = 66.09 \\ \frac{MLg}{J-J_f} K_m = 455 \end{cases} \quad (20)$$

The masses and center of mass lengths of the pendulum components were measured. The results of the measurements were: $m_r = 0.0219\text{kg}$, $m_f = 0.148\text{kg}$, $l_f = 0.151\text{m}$ and $l_r = 0.0737\text{m}$, hence $MLg = 0.2351\text{kgm}^2/\text{s}^2$.

Solving the system of equations (20), we get $K_r = 0.2712$, $K_m = 7.0878$ and $J - J_f = 0.0037\text{kg m}^2$. The relation $\frac{K_2}{R_a}$ can be obtained from (13) and (19):

$$-\frac{K_2}{R_a(J - J_f)} = -1.511 \Rightarrow \frac{K_2}{R_a} = 0.0056$$

$J_r = 0.0001672\text{kg m}^2$ and $J_f = 0.0001564\text{kg m}^2$ were estimated based on the physical properties of pendulum components.

Using the parameters calculated on the system identification, the state space representation becomes:

$$\begin{bmatrix} \dot{x}_1 \\ \dot{x}_2 \\ \dot{x}_3 \end{bmatrix} = \begin{bmatrix} 0 & 1 & 0 \\ 63.54 & -0.2712 & 0.3 \\ 0 & 0 & -7.0878 \end{bmatrix} \begin{bmatrix} x_1 \\ x_2 \\ x_3 \end{bmatrix} + \begin{bmatrix} 0 \\ -1.511 \\ 35.81 \end{bmatrix} u \quad (21)$$

$$y = [1 \ 0 \ 0] \begin{bmatrix} x_1 \\ x_2 \\ x_3 \end{bmatrix} \quad (22)$$

Considering this analysis, the transfer function of the FIP around the inverted position is given by:

$$G_{3inv} = \frac{-1.511s}{s^3 + 7.359s^2 - 61.62s - 455} \quad (23)$$

3.2 Swing-up

Two strategies of Swing-up were chosen and implemented to the system. In order to evaluate the performance of the strategies, two metrics were used: the time required to reach the Balance control range and an estimate of the amount of energy spent by the motor to implement this task.

Energy Control The first strategy adopted in this work is based on the Energy control. This approach provides a solution using a control law that uses Lyapunov's method as guidance. Åström and Furuta (2000) presented an implementation of this strategy utilizing two inverted pendulums on a cart (IPCs) as case study. Due to the intrinsic characteristics of this type of system, it was possible to accomplish the upright swing in a few swings. Nevertheless, for inertia wheel inverted pendulums, which torque is generally much lower compared to IPCs, the behavior of the system on swing-up takes too long to

complete this task when applying the same control law (Srinivas and Behera, 2008).

Lin et al. (2014) introduced a new control law, based on Energy control, proper to systems with low torque, as FIPs. The governing rule of this method is shown next:

$$v(t) = \gamma \left(\frac{1}{2} J \dot{\theta}^2 - MLg(1 + \cos(\theta)) \right) \dot{\theta} \quad (24)$$

where γ is a positive arbitrary constant. Assuming the point of maximum potential energy equals to 0 and the minimum, in the natural position, equals to $-2MgL$. For the experiments, $\gamma = 6500$ was considered.

Maximum Energy Algorithm The maximum energy algorithm consists of performing the swing-up movement in the shortest possible time, exploiting the maximum acceleration values of the actuator. Further detail about this strategy can be found in Åström and Furuta (2000).

To design the input signal, it was necessary to find the minimum number of swings the system is able to do to reach the upright position. Our FIP accomplished it in only two swings, switching the actuator three times. The saturation power was the first value sent to the motor and it was kept until the FIP reached the maximum amplitude. Then, a 0 value was sent, for a short period of time, before reversing the acceleration. At this moment, the motor is activated with maximum power in the opposite direction until the pendulum approaches the balance control region. If it is possible to reach the equilibrium position in this step, the input action is reduced aiming to reach the vertical position with reduced speed, smoothing the initial conditions for the balance control algorithm. Åström and Furuta (2000) would call this algorithm as *Double-swing triple-switch behavior* (DSTS).

3.3 Balance Control

PID controllers has been shown to be a satisfactory alternative to perform the Balance control of the FIP. Related works stated that applying only a closed loop of position control may not be enough to keep the system balanced for a long period of time. It occurs because the speed of the flywheel can progressively increase, taking the system out of stability (Almada et al., 2020). To overcome this undesired behavior, a feasible solution is to use two closed loop controllers: one for the pendulum angle and the other for the flywheel speed.

As the built FIP does not have a sensor to measure the flywheel speed, our proposed solution consists in modifying the second control loop to reduce the controller action to zero.

The gains used in the controllers were obtained combining the tuning process present in the *Control System Designer* toolbox, from *Matlab* software, and experimental tests. Initially, it was obtained a set of parameters for the FIP Angle Controller to a provide a satisfactory position control, for a short period of time. Once determined, the gains of the FIP Speed Controller were tuned. The controllers gains used on FIP were $K_{P1} = -550$, $K_{I1} = -900$ and $K_{D1} = -5$, for FIP Angle Controller, and

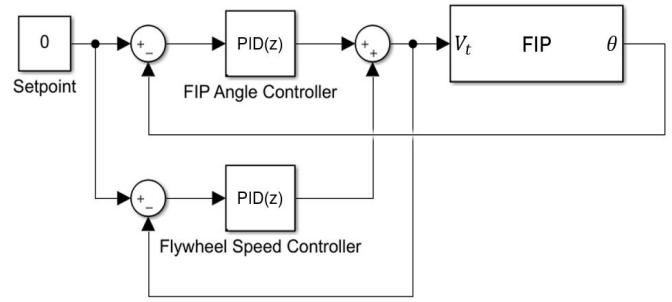


Figure 5. System control loops.

$K_{P2} = -0.04$, $K_{I2} = -1.8$ and $K_{D2} = 0$, for the flywheel speed controller. According to these parameters, the action of the angle control is much more dominant over the speed control.

3.4 Switching between Swing-up and Balancing Algorithms

The proposed system operation mainly depends on two control strategies: Swing-up and Balancing. To determine which algorithm is active, a set of rules was defined based on the spatial location of the FIP and according the concept hysteresis. Three regions in space were marked whose operation rules were previously determined, as can be seen in Figure 6.

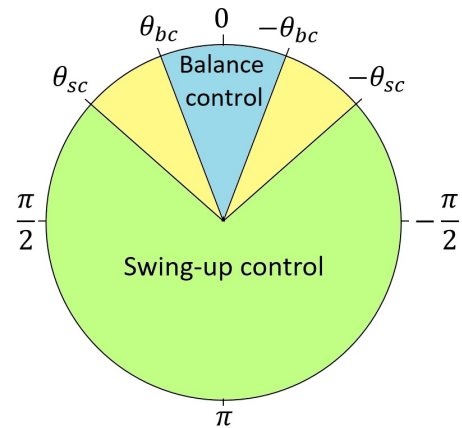


Figure 6. Algorithm selected by region.

When $|\theta| < |\theta_{bc}|$ the Balance control mode is active, when $|\theta| > |\theta_{sc}|$ the Swing-up algorithm is active. The intermediate region maintains the last active state according to the boundary angles.

Balance control if $|\theta| < |\theta_{bc}|$,
Swing-up control if $|\theta| > |\theta_{sc}|$,
keeps the last active control algorithm, otherwise.

For the implemented system, $\theta_{bc} = 0.35$ rad and $\theta_{sc} = 1.00$ rad were defined. The value of θ_{bc} was determined based on the maximum stable deflection angle, which for this FIP is approximately 0.44 rad. The purpose of making $\theta_{sc} > \theta_{bc}$ is to provide a wider range of control to the Balance controller, as its performance depends on the initial conditions of the FIP.

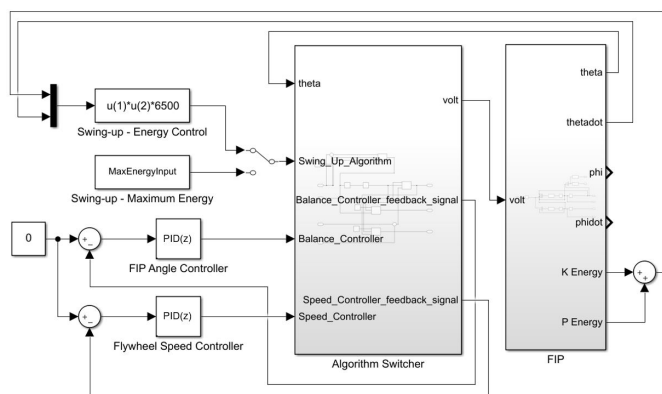


Figure 7. Simulation Architecture Design.

3.5 Simulation Architecture

A simulation environment was designed on *Simulink* to analyse the proposed strategies in this work. The non-linear model of the FIP, described by equations (7) and (8), was used to represent its behavior in the simulation environment. It was defined to grant the evaluation of the system throughout its full operating range (swing-up and stabilization). This architecture allowed to check the performance of the system when submitted to certain conditions, to enhance system response applying a fine tuning to controllers' gains and to reach a better understanding about the dynamics of the energy of the system. The simulation environment was set to operate at a sampling rate of 100Hz.

The *Algorithm Switcher* block, Figure 7, has the function of selecting the active control algorithm, according to the settings stated previously, and avoid error calculations when the Balance control is disabled. This second feature is extremely important to assure a suitable performance of the PID controllers, mainly after the switching instant.

After preliminary tests, an adjustment was implemented on the virtual model of the FIP. The parameters whose determine the system gains were multiplied by 0.73 in order to enhance the similarities with the real FIP response.

4. RESULTS AND DISCUSSIONS

4.1 Swing-up

Regarding the Swing-up strategies analyzed in this work, the results obtained from the simulations and experimentally are shown in Figure 8. The rise time of these approaches are compatible in both strategies, indicating that the non-linear model utilized on simulations has a good agreement with the real FIP. The Maximum Energy algorithm showed to be slightly faster than the Energy Control method, taking 5.2% less time to reach θ_{bc} on simulations and 7.5% less on experiments.

The control actions of each method obtained from simulations and from experiments are presented in Figures 9 and 10, respectively. There are more divergence between the signals mainly when the pendulum is reaching the position control range. The Energy control algorithm performed an undesired behavior in this region that consists in switching

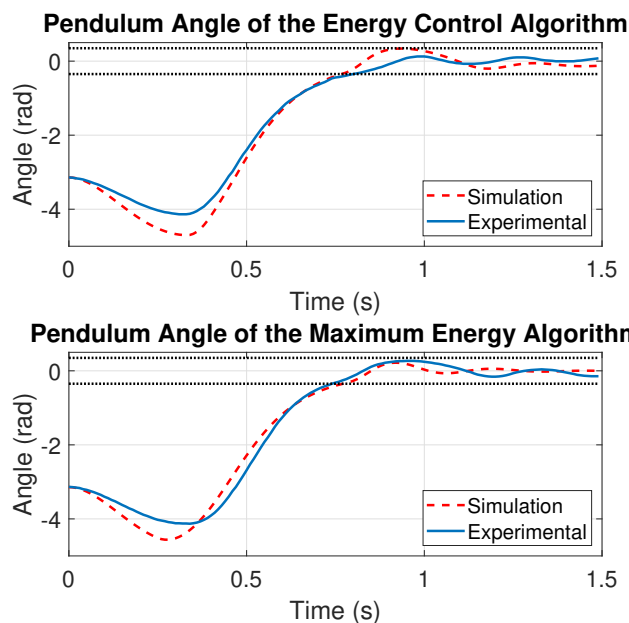


Figure 8. Swing up strategies.

the motor in a high frequency, which is not appropriate for this type of electromechanical device.

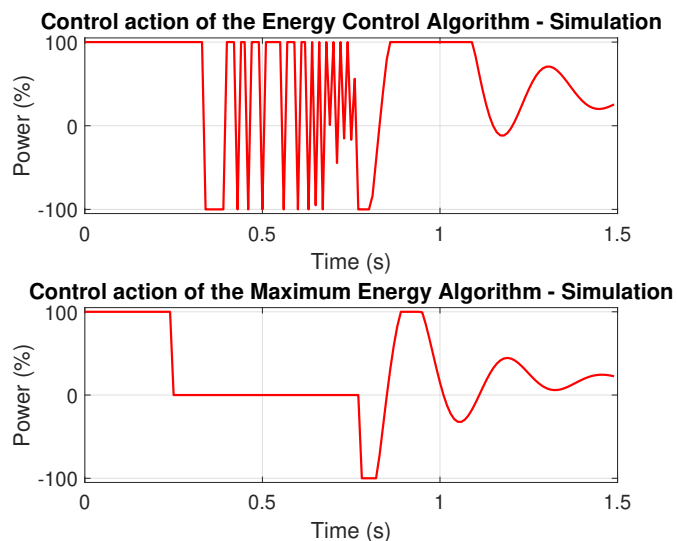


Figure 9. Swing up strategies energy comparison - Simulation.

Seeking to assess the energy demanded by each method, the area under the input signal was computed. It was used as an alternative form to estimate the efficiency between the strategies analyzed. In both cases, the Energy Control algorithm consumed more energy and took longer to perform the swing-up. Figures 11 and 12 show the results of this analysis and the vertical lines represent the switching time between the Swing-up and the Balance control algorithms. The Maximum Energy algorithm provided a better solution for this system. Besides of the best performance, the shape of the activation signal must also be considered in the analysis.

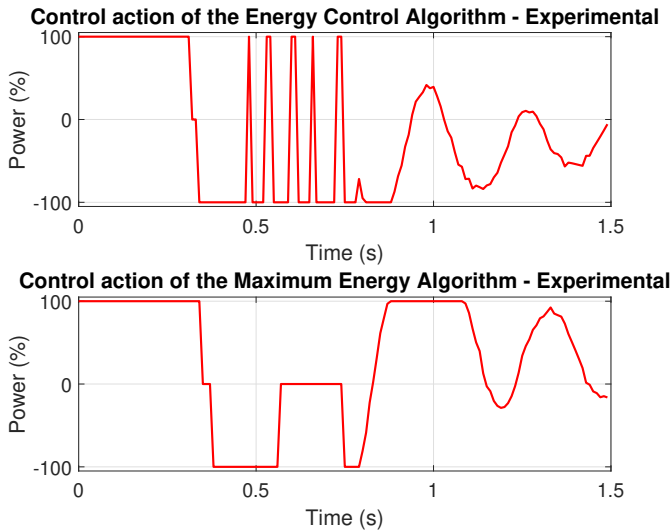


Figure 10. Swing up strategies energy comparison - Experimental.

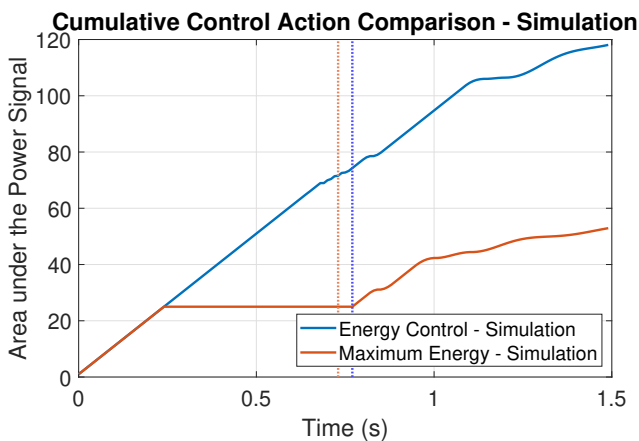


Figure 11. Swing up cumulative power - Simulation.

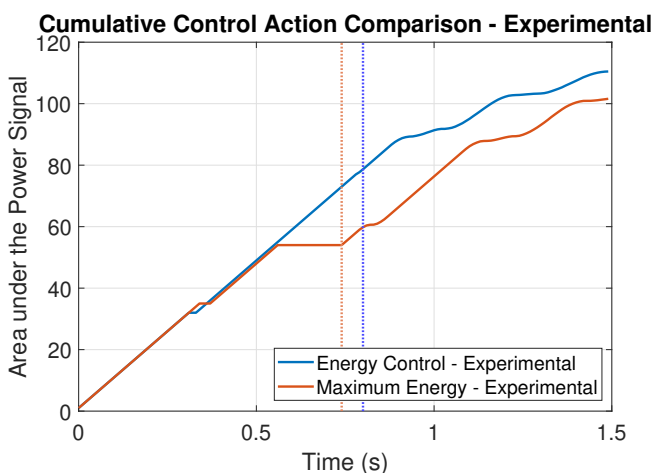


Figure 12. Swing up cumulative power - Experimental.

The speed developed by the pendulum regarding both methods can be seen in Figure 13. The vertical lines are used to mark the change of control strategies. The Energy Control algorithm reached the Balance Control range with

a lower speed than the other method, such on simulations and experimentally.

All the experiments were carried out considering a sampling frequency of 100Hz. This frequency value was chosen taking the natural frequency of the system and the hardware capabilities into account.

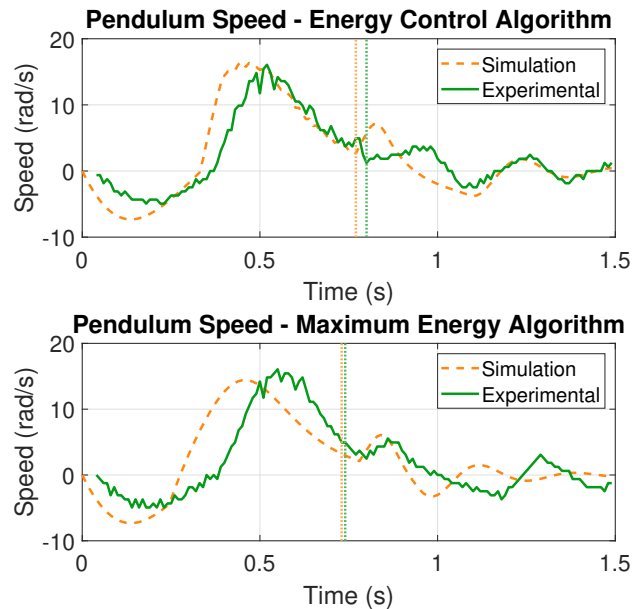


Figure 13. Swing up speed - Comparison.

The Swing-up algorithms were tested considering non-zero initial conditions in order to evaluate the robustness of the techniques. For this, the motor was activated with 20% of power for 2 second, then the Swing-up control was enabled. This experiment was performed 5 times for each algorithm. The Energy Control technique obtained success in all trials, while the Maximum Energy algorithm failed only once. Additional tests were performed providing more energy to the system in order to move the pendulum further away from the initial resting conditions. Therefore, the motor was activated for a longer period (2s) and turned off for 1s, before switching to its respective control law. The results obtained in these experiments showed that the Energy Control algorithm has a good ability to withstand variations in the initial conditions of the FIP. Furthermore, the Maximum Energy algorithm did not present the same resilience, it was only successful when very low perturbation was applied.

The analysis of the results reinforces that the closed-loop technique showed greater robustness when starting the operation with the FIP out of the rest conditions. Further experiments can be performed to evaluate the limit values of the initial conditions which will impact substantially on the suitable system operation.

4.2 Balance Control

Figure 14 shows the FIP working for a period of 10 seconds, considering the Swing-up techniques analyzed in this work. Although both methods stabilized the FIP at the reference position, the Maximum Energy algorithm

smoothed the initial conditions of Balance control and reduced the oscillations of the FIP angle and the control signal. This behavior might turn the system more robust against disturbances.

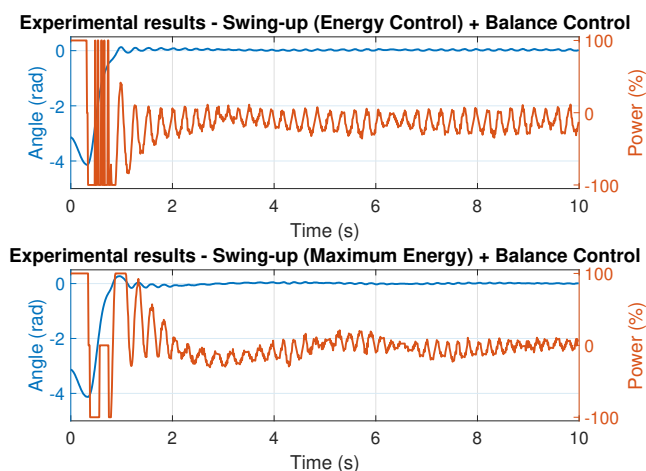


Figure 14. System behavior.

Calculating the cumulative error only at region where the Balance control is active, we get $E_{EC} = 30.33$ and $E_{ME} = 29.77$, to swing-up algorithms of Energy Control and Maximum Energy, respectively. Although the magnitude of the difference between these values is small, there is a notable contrast on error trends.

Further experiments have demonstrated a suitable performance of the FIP to resist around the equilibrium position when small disturbances were applied to the system.

5. CONCLUSION

The study of underactuated systems is still a field of research that has been extensively explored in engineering. Inverted pendulums are an important case of this class of systems. This work presented a flywheel inverted pendulum design, capable of performing the Swing-up and the Balance control.

A FIP prototype was built to perform the analysis of this work. System Identification experiments were carried out to obtain a transfer function to represent accordingly the real system. The FIP modeling was performed considering the voltage applied to the DC motor as the input parameter of the transfer function. This choice allowed to obtain a more reasonable model, providing greater reliability to the analysis when compared with models that consider torque as input signal, which is only valid under specific conditions. From the function obtained experimentally, it was possible to implement a FIP model in a simulation environment with great similarity to the prototype.

Two energy-based Swing-up algorithms were analyzed according to some specific metrics. The Maximum Energy algorithm proved to be faster and consumed less energy than the Energy Control algorithm, such on simulations and on experiments. However, the Energy Control technique proved to be more resilient to guarantee the proper functioning of the system even when the pendulum starts from non-zero initial conditions.

Balance control was satisfactorily achieved through the implementation of two PID control loops, regarding to both swing-up strategies assessed in this work. It was evident the impact of swing-up performance on determining the initial conditions of the balancing stage. Switching algorithms with suitable energy levels is essential to stabilize faster and improve the robustness of the system. The Maximum Energy algorithm was able to provide better conditions to the Balance controller that resulted in a lower steady-state error when compared to the Energy Control algorithm.

REFERENCES

- Almada, J., Frizon, L., Kolling Dutra, M., and Milhomem, R. (2020). Aspectos práticos sobre o desenvolvimento de um pêndulo invertido com roda de reação. In *Congresso Brasileiro de Automática*.
- Dai, F., Gao, X., Jiang, S., Guo, W., and Liu, Y. (2015). A two-wheeled inverted pendulum robot with friction compensation. *Mechatronics*, 30, 116–125.
- Ferrante, R. (2017). *A Robust Control Approach for Rocket Landing*. Master's thesis, University of Edinburgh.
- Kareem, A. (1983). Nonlinear dynamic analysis of compliant offshore platforms subjected to fluctuating wind. *Journal of Wind Engineering and Industrial Aerodynamics*, 14, 345–356.
- Lin, J., Chen, S., and Gau, W.H. (2014). Design and implementation of a novel inertia flywheel pendulum mechatronic kit. *Journal of Vibration and Control*, 21.
- Nguyen, T.S. and Huynh, T.H. (2016). Study on a two-loop control architecture to balance an inertia wheel pendulum. In *3rd National Foundation for Science and Technology Development Conference on Information and Computer Science (NICCS)*.
- Olivares, M. and Albertos, P. (2013). On the linear control of underactuated systems: The flywheel inverted pendulum. In *2013 10th IEEE International Conference on Control and Automation (ICCA)*, 27–32.
- Spong, M.W., Corke, P., and Lozano, R. (2001). Nonlinear control of the reaction wheel pendulum. *Automatica*, 37(11), 1845–1851.
- Srinivas, K. and Behera, L. (2008). Swing-up control strategies for a reaction wheel pendulum. *Int. J. Systems Science*, 39, 1165–1177.
- Teja, G.P., Dhabale, A., and Waghmare, T. (2020). Non-linear control of the reaction wheel pendulum using passivity-based control and backstepping control. In *2020 IEEE First International Conference on Smart Technologies for Power, Energy and Control (STPEC)*, 1–6.
- Trentin, J.F.S., Da Silva, S., De Souza Ribeiro, J.M., and Schaub, H. (2020). Inverted pendulum nonlinear controllers using two reaction wheels: Design and implementation. *IEEE Access*, 8, 74922–74932.
- Vasconcelos, J.R.C., González, E.M.A., and Del Foyo, P.M.G. (2019). Design and control of a flywheel inverted pendulum system. In *Congresso Brasileiro de Automática*, volume 1.
- Åström, K. and Furuta, K. (2000). Swinging up a pendulum by energy control. *Automatica*, 36(2), 287–295.